An Optimized Any-Cell-to-Any-Cell Equalizer Based on Coupled Half-Bridge Converters for Series-Connected Battery Strings

Yunlong Shang, *Member, IEEE*, Naxin Cui, *Senior Member, IEEE*, and Chenghui Zhang, *Senior Member, IEEE*

***Abstract*—An optimized automatic equalizer based on coupled half-bridge converters using a multi-winding transformer is proposed for series-connected battery packs. The proposed equalizer not only reduces the transformer windings by half, achieving a compact size and low cost, but also realizes the automatic any-cell-to-any-cell equalization, significantly speeding up the equalization process. The expressions of the equalization current and efficiency are derived and verified by experimental results. The design considerations of the switching frequency and the magnetic inductance are analyzed and discussed to optimize the equalization current and efficiency. The maximum balancing efficiency of 95% is realized at the switching frequency of 5 kHz and the balancing power of 0.85 W. Comparative experimental studies of the proposed equalizer with the forward–flyback solution are conducted to validate that the balancing performances of the proposed equalizer are unaffected by the reduced transformer windings.**

***Index Terms*—Electric vehicles, equalizers, half-bridge converters, Li-Ion batteries, multi-winding transformers.**

I. Introduction

SERIES-CONNECTED lithium-ion (Li-Ion) battery strings have relative consistency but absolute inconsistency [1], [2]. Therefore, many battery balancing methods have been proposed to ensure series-connected batteries consistently charged and discharged to improve the useful capacity and life of battery packs [3], [4].

Due to the small size and low cost, the passive equalizer only uses one small resistor and one switch for one cell, which is widely applied in electric vehicles (EVs) [1]. Shang *et al*. [5] introduced an integrated heater-equalizer, which not only realizes

Manuscript received August 28, 2018; revised November 1, 2018; accepted December 10, 2018. Date of publication December 18, 2018; date of current version June 10, 2019. This work was supported in part by the Key Project of National Natural Science Foundation of China under Grant 61633015, in part by the Major Scientific Instrument Development Program of the National Natural Science Foundation of China under Grant 61527809, and in part by the National Natural Science Foundation of China under Grant U1764258. Recommended for publication by Associate Editor F. H. Khan. *(Corresponding author: Chenghui Zhang.)*

Y. Shang is with the School of Control Science and Engineering, Shandong University, Jinan 250061, China, and also with the Department of Electrical and Computer Engineering, San Diego State University, San Diego, CA 92182 USA (e-mail:

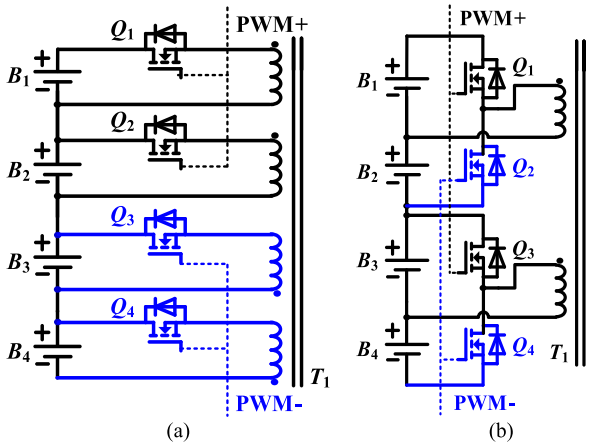

Fig. 1. Comparison of the multi-winding transformer-based equalizers. (a) Conventional forward–flyback equalizer [26]. (b) Proposed equalizer based on coupled half-bridge converters.

voltage monitoring. In a similar case, Uno and Kukita [24] proposed the simultaneous P2C equalizers based on voltage multiplier. It is worth noting that the C2P and P2C methods have a low equalization efficiency, i.e., 80%-85%, because of the loop current.

In order to improve the equalization efficiency, Li *et al*. [15] introduced a simultaneous any-cell-to-any-cell (AC2AC) topology based on forward operation. This method only requires n MOSFETs and n windings for n cells to realize the simultaneous equalization among all the cells, leading to a compact size and high equalization speed. However, this equalizer requires additional demagnetizing circuits to absorb the energy stored in the transformer, leading to a complex design and low reliability. In order to remove the demagnetizing circuits, Shang *et al*. [26] designed a forward–flyback equalizer shown in Fig. 1(a), which has almost the same circuit configuration with the forward-conversion one [15]. The biggest difference is that the transformer windings are divided into two groups, which have the opposite polarities. The equalization in one group is obtained based on forward operation and the equalization between the two groups is realized based on flyback conversion. It is worth noting that the demagnetization for the transformer is automatically realized by the flyback conversion without using demagnetizing circuits, resulting in a simple control and high reliability. Furthermore, Shang *et al*. [27] proposed a modularized architecture based on the forward–flyback equalizer [26]. The highlighted advantage is that only one equalization circuit is shared by the equalization in and among battery modules.

In order to further reduce the volume of the transformers and improve the balancing efficiency, this paper proposes an automatic equalizer based on coupled half-bridge converters, which can realize the simultaneous AC2AC equalization for all cells. This paper has four original contributions. First, the number of the transformers is reduced by half, contributing to a compact size and comparatively low price. Second, the analytical expressions of the balancing current and efficiency are derived and verified by experiments. Third, the proposed equalizer is analyzed and discussed at different switching frequencies and the magnetic inductances to provide a guidance for optimizing the balancing current and efficiency. Finally, an experimental comparison of the proposed solution with the traditional forward–flyback equalizer [26] is conducted to prove that the outstanding equalization performances are not affected by the reduced windings.

II. Proposed Equalizer

A. Circuit Configuration

Fig. 1(b) shows the optimized automatic equalizer based on coupled half-bridge converters for four cells. It can be seen that one cell needs one MOSFET and two cells share one transformer winding, which form a conventional half-bridge converter. Moreover, all the half-bridge converters are coupled by a multi-winding transformer. It is worth mentioning that each winding has the same turn number to achieve the equalization among the odd/even cells. Compared with the forward–flyback equalizer [26] shown in Fig. 1(a), the proposed equalizer only needs half of the transformer windings, significantly reducing the volume and cost of the equalizer.

B. Operation Principles

Like the conventional forward–flyback equalizer [26], the proposed equalizer only requires two complementary pulsewidth modulations (PWMs) with a 50% duty cycle to drive the odd and even MOSFETs. Fig. 2 shows the operational principles under the initial cell voltages of $V_{B1} > V_{B2} > V_{B3} > V_{B4}$. Fig. 3 shows the theoretical key waveforms. It can be noted that the proposed topology has six working states within one switching period.

State I [$t_0 - t_1$, Fig. 2(a)]: MOSFETs Q_1 and Q_3 are turned ON at t_0. According to Faraday's law, i_1 continues to flow out of the transformer, charging cell B_1. i_2 continues to flow into the transformer, discharging cell B_3. The magnetic inductor L_m is charged by B_3, which resets the transformer.

State II [$t_1 - t_2$, Fig. 2(b)]: Due to the highest voltage of B_1, i_1 increases first to zero at t_1. B_1 starts to discharge to the transformer. In this state, the magnetic inductor L_m is simultaneously charged by B_1 and B_3.

State III [$t_2 - t_3$, Fig. 2(c)]: At t_2, i_2 decreases to zero. B_3 starts to be charged by the transformer, and B_1 continues to discharge to the transformer and charge magnetic inductor L_m. This state achieves the equalization between B_1 and B_3 based on forward conversion.

It is important to note that the magnetizing current i_{Lm} increases linearly because the higher voltage cells charge the magnetic inductor during States I–III.

State IV [$t_3 - t_4$, Fig. 2(d)]: Q_2 and Q_4 are turned ON at t_3. Based on Faraday's law, i_1 and i_2 continue to flow as the last state, which resets the energy stored in the magnetic inductor. It can be seen that B_2 is simultaneously charged by the magnetic inductor L_m and B_4.

State V [$t_4 - t_5$, Fig. 2(e)]: Due to the lowest voltage of B_4, i_2 increases first to zero at t_4. B_4 starts to be charged by the

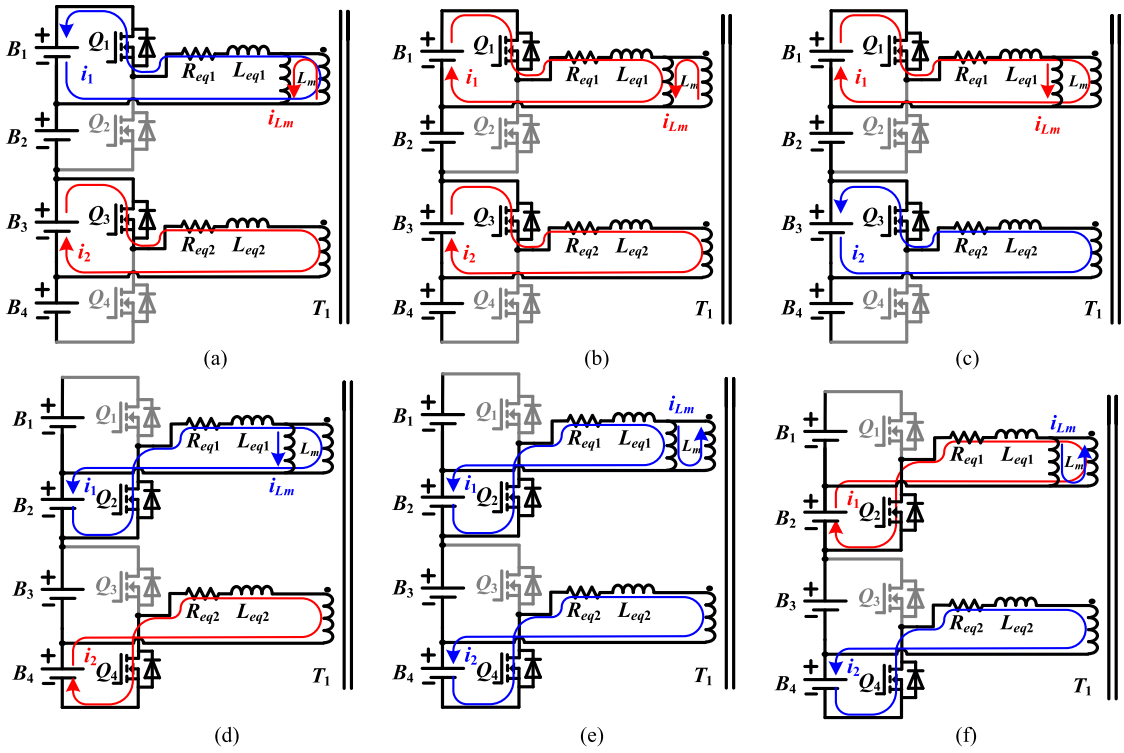

Fig. 2. Operational principles under the assumption of $V_{B1} > V_{B2} > V_{B3} > V_{B4}$. (a) State I. (b) State II. (c) State III. (d) State IV. (e) State V. (f) State VI.

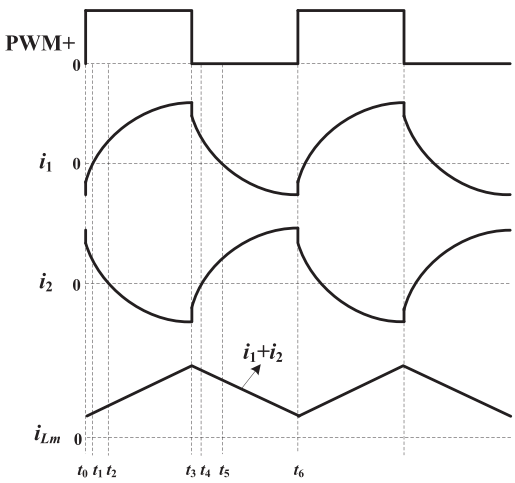

Fig. 3. Theoretical waveforms of the balancing and magnetizing currents.

transformer. In this state, B_2 and B_4 are simultaneously charged by the magnetic inductor L_m.

State VI [$t_5 - t_6$, Fig. 2(f)]: At t_5, i_1 decreases to zero. B_2 starts to discharge to the transformer, and B_4 is charged by B_2 and the magnetic inductor L_m. This state achieves the equalization between B_2 and B_4 based on forward conversion.

It is worth mentioning that during States IV–VI, the magnetizing current $i_1 + i_2$ decreases linearly because the magnetic inductor charges the lower voltage cells. Therefore, the equalization between the odd cells B_1, B_3 and the even cells B_2, B_4 is achieved based on flyback conversion.

It can be noted that the equalization between adjacent two cells B_1, B_2 and B_3, B_4 is also automatically achieved based on buck–boost conversion during the two complementary states.

According to the six working states, it can be noted that the proposed topology realizes the automatic and direct AC2AC equalization based on forward, flyback, and buck–boost conversions.

C. Modeling and Analysis of the Magnetizing and Balancing Currents

According to Kirchhoff's voltage law, the balancing currents of the two half-bridge converters during the first half period can be expressed as follows:

$$(L_m + L_f) \cdot \frac{di_1}{dt} + L_m \cdot \frac{di_2}{dt} = V_{B1} - i_1 R_{\text{eq}}, 0 < t < \frac{T}{2} \tag{1}$$

$$(L_m + L_f) \cdot \frac{di_2}{dt} + L_m \cdot \frac{di_1}{dt} = V_{B3} - i_2 R_{\text{eq}}, 0 < t < \frac{T}{2} \tag{2}$$

where i_1 and i_2 are the balancing currents flowing though the two half-bridge converters, respectively. R_{eq} represents the equivalent resistance, including the on resistance of a MOSFET R_{on}, the connecting resistance R_c, and the winding resistance R_w. L_m is the magnetic inductance. L_f is the leakage inductance. T is the switching period.

Adding (2) with (1) yields the expression for the magnetizing current $i_1 + i_2$ during the first half period

$$(2L_m + L_f) \cdot \frac{d(i_1 + i_2)}{dt} + (i_1 + i_2) \cdot R_{\text{eq}} - (V_{B1} + V_{B3}) = 0, 0 < t < \frac{T}{2}. \tag{3}$$

Analogously, the magnetizing current during the second half period can be expressed as follows:

$$(2L_m + L_f) \cdot \frac{d(i_1 + i_2)}{dt} + (i_1 + i_2) \cdot R_{\text{eq}} + (V_{B2} + V_{B4}) = 0, \frac{T}{2} < t < T. \tag{4}$$

By solving (3) and (4) with $i_1(0) + i_2(0) = i_1(T) + i_2(T)$ and $i_1(\frac{T}{2}^-) + i_2(\frac{T}{2}^-) = i_1(\frac{T}{2}^+) + i_2(\frac{T}{2}^+)$, the magnetizing current can be deduced as, respectively

$$\begin{cases} i_{Lm}(t) = i_1(t) + i_2(t) = \frac{V_{B1}+V_{B3}}{R_{\text{eq}}} \\ -\frac{V_{B1}+V_{B2}+V_{B3}+V_{B4}}{R_{\text{eq}}} \cdot \frac{1}{e^{-\frac{R_{\text{eq}}}{2L_m+L_f}\cdot\frac{T}{2}}+1} \cdot e^{-\frac{R_{\text{eq}}}{2L_m+L_f}\cdot t}, \\ \quad 0 < t < \frac{T}{2} \\ i_{Lm}(t) = i_1(t) + i_2(t) = -\frac{V_{B2}+V_{B4}}{R_{\text{eq}}} + \\ \frac{V_{B1}+V_{B2}+V_{B3}+V_{B4}}{R_{\text{eq}}} \cdot \frac{1}{e^{-\frac{R_{\text{eq}}}{2L_m+L_f}\cdot\frac{T}{2}}+1} \cdot e^{-\frac{R_{\text{eq}}}{2L_m+L_f}\cdot\left(t-\frac{T}{2}\right)}, \\ \quad \frac{T}{2} < t < T. \end{cases} \tag{5}$$

Due to $L_m \gg L_f$, $-\frac{R_{\text{eq}}}{2L_m+L_f} \cdot t \to 0$, and $e^{-\frac{R_{\text{eq}}}{2L_m+L_f}\cdot\frac{T}{2}} \approx 1$, (5) can be simplified as follows:

$$\begin{cases} i_{Lm}(t) \approx \frac{V_{B1}+V_{B3}-V_{B2}-V_{B4}}{2R_{\text{eq}}} + \frac{V_{B1}+V_{B2}+V_{B3}+V_{B4}}{4L_m} \\ \quad \cdot t, 0 < t < \frac{T}{2} \\ i_{Lm}(t) \approx \frac{V_{B1}+V_{B3}-V_{B2}-V_{B4}}{2R_{\text{eq}}} - \frac{V_{B1}+V_{B2}+V_{B3}+V_{B4}}{4L_m} \\ \quad \cdot\left(t-\frac{T}{2}\right), \frac{T}{2} < t < T. \end{cases} \tag{6}$$

It can be seen that increasing the magnetic inductance or the switching frequency can decrease the peak magnetizing current, reducing the core loss of the transformer.

Based on (6), the voltage across the magnetic inductance can be presented by the following equation:

$$V_{Lm} = \frac{V_{B1} + V_{B2} + V_{B3} + V_{B4}}{4}. \tag{7}$$

According to Kirchhoff's voltage law, the equalization currents during the first half period can be expressed as, respectively

$$\begin{cases} L_f \frac{di_1}{dt} + i_1 R_{\text{eq}} = \frac{3V_{B1}-V_{B2}-V_{B3}-V_{B4}}{4} \\ L_f \frac{di_2}{dt} + i_2 R_{\text{eq}} = \frac{3V_{B3}-V_{B1}-V_{B2}-V_{B4}}{4}. \end{cases}, 0 < t < \frac{T}{2} \tag{8}$$

Analogously, the balancing currents during the second half period can be expressed as, respectively

$$\begin{cases} L_f \frac{di_1}{dt} + i_1 R_{\text{eq}} = \frac{V_{B1}+V_{B3}+V_{B4}-3V_{B2}}{4} \\ L_f \frac{di_2}{dt} + i_2 R_{\text{eq}} = \frac{V_{B1}+V_{B2}+V_{B3}-3V_{B4}}{4}. \end{cases}, \frac{T}{2} < t < T \tag{9}$$

According to (8) and (9), the equalization currents can be solved as, respectively

$$\begin{cases} i_1(t) = \frac{3V_{B1}-V_{B2}-V_{B3}-V_{B4}}{4R_{\text{eq}}} - \\ \frac{V_{B1}-V_{B3}+V_{B2}-V_{B4}}{2R_{\text{eq}}} \cdot \frac{1}{e^{-\frac{R_{\text{eq}}}{L_f}\cdot\frac{T}{2}}+1} \cdot e^{-\frac{R_{\text{eq}}}{L_f}t} \\ i_2(t) = \frac{3V_{B3}-V_{B1}-V_{B2}-V_{B4}}{4R_{\text{eq}}} + \\ \frac{V_{B1}-V_{B3}+V_{B2}-V_{B4}}{2R_{\text{eq}}} \cdot \frac{1}{e^{-\frac{R_{\text{eq}}}{L_f}\cdot\frac{T}{2}}+1} \cdot e^{-\frac{R_{\text{eq}}}{L_f}t} \end{cases}, 0 < t < \frac{T}{2} \tag{10}$$

$$\begin{cases} i_1(t) = \frac{V_{B1}+V_{B3}+V_{B4}-3V_{B2}}{4R_{\text{eq}}} + \\ \frac{V_{B1}-V_{B3}+V_{B2}-V_{B4}}{2R_{\text{eq}}} \cdot \frac{1}{e^{-\frac{R_{\text{eq}}}{L_f}\cdot\frac{T}{2}}+1} \cdot e^{-\frac{R_{\text{eq}}}{L_f}\left(t-\frac{T}{2}\right)} \\ i_2(t) = \frac{V_{B1}+V_{B2}+V_{B3}-3V_{B4}}{4R_{\text{eq}}} - \\ \frac{V_{B1}-V_{B3}+V_{B2}-V_{B4}}{2R_{\text{eq}}} \cdot \frac{1}{e^{-\frac{R_{\text{eq}}}{L_f}\cdot\frac{T}{2}}+1} \cdot e^{-\frac{R_{\text{eq}}}{L_f}\left(t-\frac{T}{2}\right)}. \end{cases}, \frac{T}{2} < t < T \tag{11}$$

Based on (10) and (11), the average balancing currents of the cells can be calculated as, respectively

$$\begin{cases} I_{B1} \approx \frac{1}{R_{\text{eq}}} \cdot \left(\frac{3V_{B1}-V_{B2}-V_{B3}-V_{B4}}{8} - \frac{L_f}{T} \cdot \frac{V_{B1}-V_{B3}+V_{B2}-V_{B4}}{2 \cdot R_{\text{eq}}}\right) \\ I_{B2} \approx \frac{1}{R_{\text{eq}}} \cdot \left(\frac{3V_{B2}-V_{B1}-V_{B3}-V_{B4}}{8} - \frac{L_f}{T} \cdot \frac{V_{B1}-V_{B3}+V_{B2}-V_{B4}}{2 \cdot R_{\text{eq}}}\right) \\ I_{B3} \approx \frac{1}{R_{\text{eq}}} \cdot \left(\frac{3V_{B3}-V_{B1}-V_{B2}-V_{B4}}{8} + \frac{L_f}{T} \cdot \frac{V_{B1}-V_{B3}+V_{B2}-V_{B4}}{2 \cdot R_{\text{eq}}}\right) \\ I_{B4} \approx \frac{1}{R_{\text{eq}}} \cdot \left(\frac{3V_{B4}-V_{B1}-V_{B2}-V_{B3}}{8} + \frac{L_f}{T} \cdot \frac{V_{B1}-V_{B3}+V_{B2}-V_{B4}}{2 \cdot R_{\text{eq}}}\right). \end{cases} \tag{12}$$

It can be observed that the equalization current is in inverse proportion to the equivalent resistance R_{eq}. The larger the cell voltage difference, the larger the balancing current. Particularly, decreasing the switching frequency or the leakage inductance can improve the average equalization current. It is worth mentioning that the cell equalization current is independent of the magnetic inductance. According to (7) and (12), it can be seen that the leakage inductance only affects the balancing current rather than the balanced cell voltage.

D. Balancing Loss and Efficiency Analysis

The balancing dissipation mainly includes the conduction, core, and switching losses.

The conduction loss due to the equivalent resistance in circuits can be expressed as follows:

$$P_D = \left(I_{B1}^2 + I_{B2}^2 + I_{B3}^2 + I_{B4}^2\right) \cdot R_{\text{eq}}. \tag{13}$$

It can be seen that the conduction loss will increase with the decrease of the switching frequency due to the increased balancing current according to (12). However, due to the skin effect, the equivalent resistance will increase with the increase of the switching frequency, potentially increasing the conduction loss.

The core loss of the transformer can be calculated by Steinmetz equation as follows [28], [29]:

$$P_C = k \cdot f^a \cdot \Delta B^b = k \cdot f^a \cdot \left(\frac{L_m}{As \cdot N} \cdot \Delta I_{Lm} \right)^b \quad (14)$$

where f is the switching frequency. ΔB is the peak-to-peak flux density. k, a, and b are the Steinmetz coefficients, which can be determined from the manufacturers. A_S is the cross-sectional area of the magnetic core. N is the turns number. ΔI_{Lm} is the peak-to-peak magnetizing current, which can be achieved according to (6)

$$\Delta I_{Lm} = \frac{V_{B1} + V_{B2} + V_{B3} + V_{B4}}{8 L_m \cdot f}. \quad (15)$$

Substituting (15) into (14), the core loss can be further deduced as follows:

$$P_C = k \cdot f^{a-b} \cdot \left(\frac{V_{B1} + V_{B2} + V_{B3} + V_{B4}}{8As \cdot N} \right)^b. \quad (16)$$

Due to $a < b$, the core loss will decrease with the increase of the switching frequency. Increasing the cross-sectional area or the turns number will also decrease the core loss. However, the cross-sectional area is limited by the size of the transformer. Therefore, the turns number as well as the magnetic inductance should be as large as possible to decrease the core loss.

The switching loss of the MOSFETs can be represented by the following [30], [31]:

$$P_S = \sum_{i=1}^{n} \left(\frac{1}{2} f \cdot C_{\mathrm{DS}} \cdot V_{Bi}^2 + \frac{1}{2} f \cdot V_B \cdot I_{Bi} \cdot t_f \right) \quad (17)$$

where n is the cell number. C_{DS} is the MOSFET drain–source capacitance. t_f is the MOSFET fall time.

According to (13)–(17), the balancing efficiency can be expressed as follows:

$$\eta = \frac{P_{\mathrm{out}}}{P_{\mathrm{out}} + P_D + P_C + P_S} \times 100\% \quad (18)$$

where P_{out} is the output balancing power. According to the above analyses, with the increase of the switching frequency, the switching loss will increase. With the decrease of the switching frequency, the conduction and core losses will increase. Therefore, an optimized switching frequency can be achieved to fairly balance the conduction, core, and switching losses for the minimum total loss.

III. Experimental Results

Fig. 4 illustrates the experimental setup for four series-connected Li-Ion batteries with 1100 mAh capacity. CSD19535KCS MOSFETs are used for $Q_1 - Q_4$. A YOKOGAWA WT1800 Precision Power Analyzer has been used to measure the charge or discharge power of each cell. The balancing efficiency is determined by dividing the total cell charge power by the total cell discharge power [9]. The detailed mathematical expressions can be found in [9]. Table I illustrates the magnetic inductances, leakage inductances, and equivalent resistances of the multi-winding transformers with different turns number.

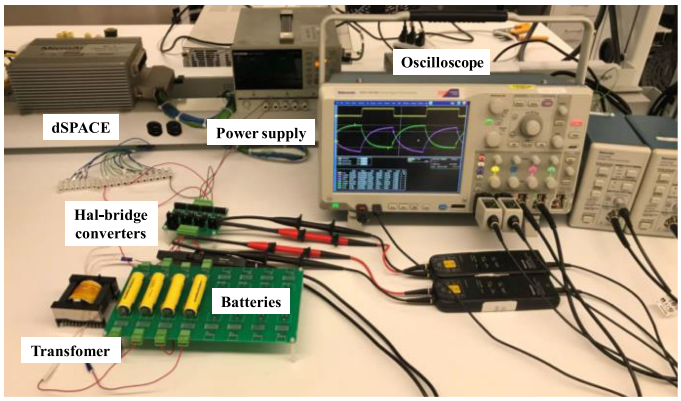

Fig. 4. Photograph of the experimental setup.

TABLE I
Parameters of Multi-Winding Transformers

Turns number N	L_m (μH)	L_f (μH)	R_w (mΩ)
10	129	1.59	39
11.5	170	1.48	39
15	287	1.45	40
20	508	1.2	41

Note: R_w is the winding resistance.

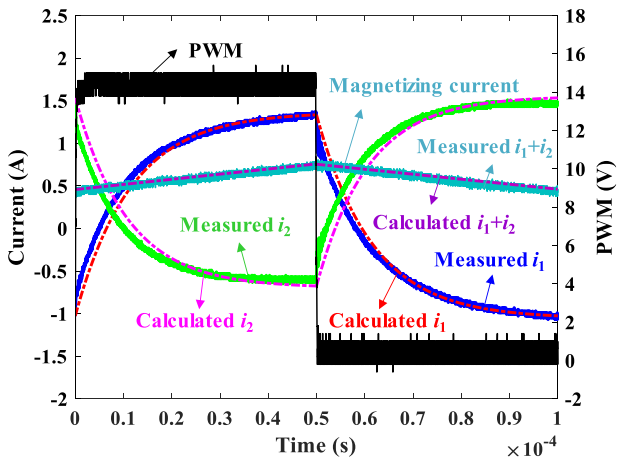

Fig. 5. Waveforms of the balancing and magnetizing currents at 10 kHz.

Fig. 5 illustrates the waveforms of the balancing and magnetizing currents at 10 kHz under the initial voltage distribution of $V_{B1} > V_{B2} > V_{B3} > V_{B4}$. Due to the larger magnetic inductance, the measured magnetizing current $i_1 + i_2$ is a sawtooth waveform with the average value of 0.59 A. Nevertheless, the balancing currents i_1 and i_2 are approximately exponential waveforms, which are mainly decided by the leakage inductance and equivalent resistance. It is important to note that the calculated currents match well with the experimental waveforms, which verifies (6) and (11).

Fig. 6 shows the measured average balancing currents with different switching frequencies and magnetic inductances, respectively. We can observe that the equalization current is approximately proportional to the voltage difference. As shown in

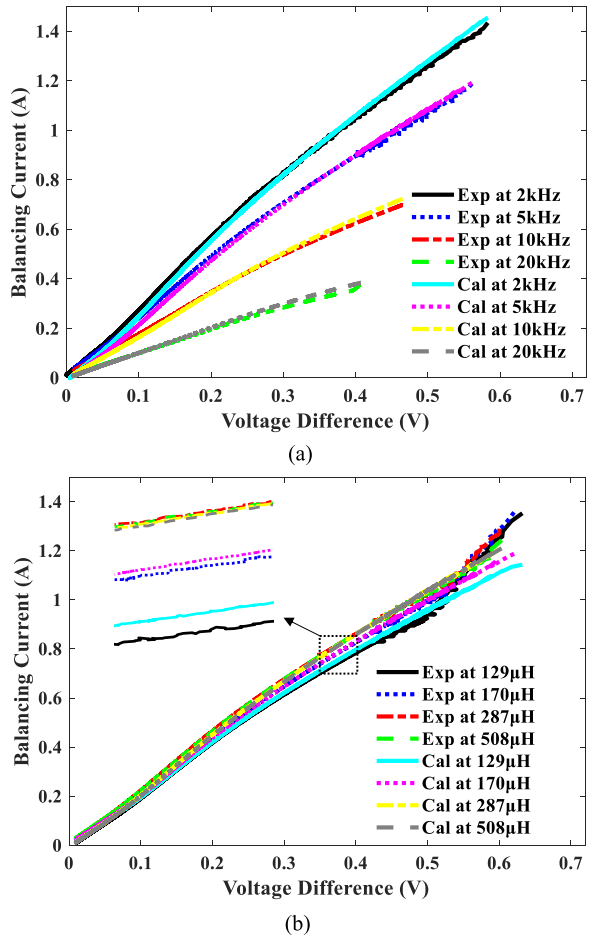

Fig. 6. Average balancing currents. (a) At different switching frequencies with the magnetic inductance of 287 μH. (b) With different magnetic inductances at 5 kHz.

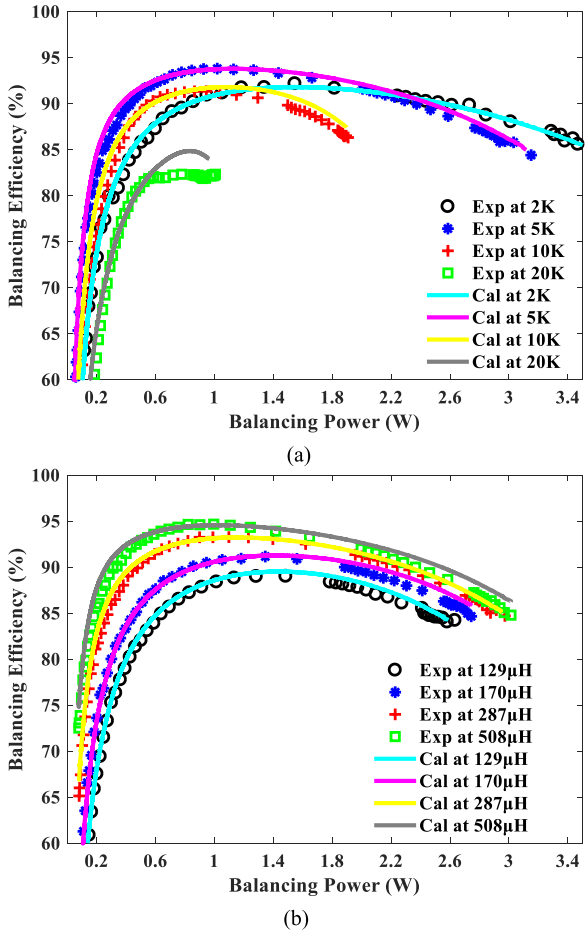

Fig. 7. Equalizing efficiencies. (a) At different switching frequencies with the magnetic inductance of 287 μH. (b) With different magnetic inductances at 5 kHz.

Fig. 6(a), the equalization current can be dramatically improved by decreasing the switching frequency. As shown in Fig. 6(b), the equalization current is independent of the magnetic inductance. It is worth mentioning that the small difference among the currents is mainly caused by the different equivalent resistances and leakage inductances at different magnetic inductances. In summary, the calculated equalization currents agree well with the measured currents at different switching frequencies and magnetic inductances, which proves (12).

Fig. 7 shows the measured equalization efficiencies with different switching frequencies and magnetic inductances, respectively. As shown in Fig. 7(a), it can be observed that the highest efficiency curve is obtained at 5 kHz. However, when the switching frequency decreases to 2 kHz, the efficiency also decreases because of the increasing copper and core losses of the transformer. Particularly, the equalization efficiency dramatically decreases as the switching frequency increases to 20 kHz due to the larger switching loss. As shown in Fig. 7(b), the balancing efficiency can be significantly improved by increasing the magnetic inductance or the turns number at the same switching frequency. In summary, the measured peak efficiency is about 95% at the switching frequency of 5 kHz and the equalization power of 0.85 W with the magnetic inductance of 508 μH. We can observe that the calculated equalization efficiencies are consistent with the measured ones at different switching frequencies and magnetic inductances, which proves the validity of (13)–(18).

Fig. 8 presents the voltage evolutions with the proposed equalizer under different initial cell voltages. From Fig. 8(a) and (c), it can be observed that all the cells can be simultaneously equalized regardless of the cell voltage distributions. This proves that the proposed equalizer is robust to the initial imbalanced cell voltages because of the AC2AC balancing characteristic. As shown in Fig. 8(b) and (d), the equalization currents depend on the cell voltage difference. The larger the cell voltage difference, the larger the balancing currents. The balancing currents will approach to zero as the cell voltage difference becomes zero, showing the convergence of the proposed equalizer.

In order to show the applicability of the proposed topology, Fig. 9 presents the balancing results for three series-connected cells. We can observe that the cell voltages are balanced and the equalization currents become zero after 2000 s. This verifies that the proposed topology can be also applied to odd series-connected cells.

Fig. 10 shows the balancing results of the conventional forward–flyback equalizer [26] with the same initial condition

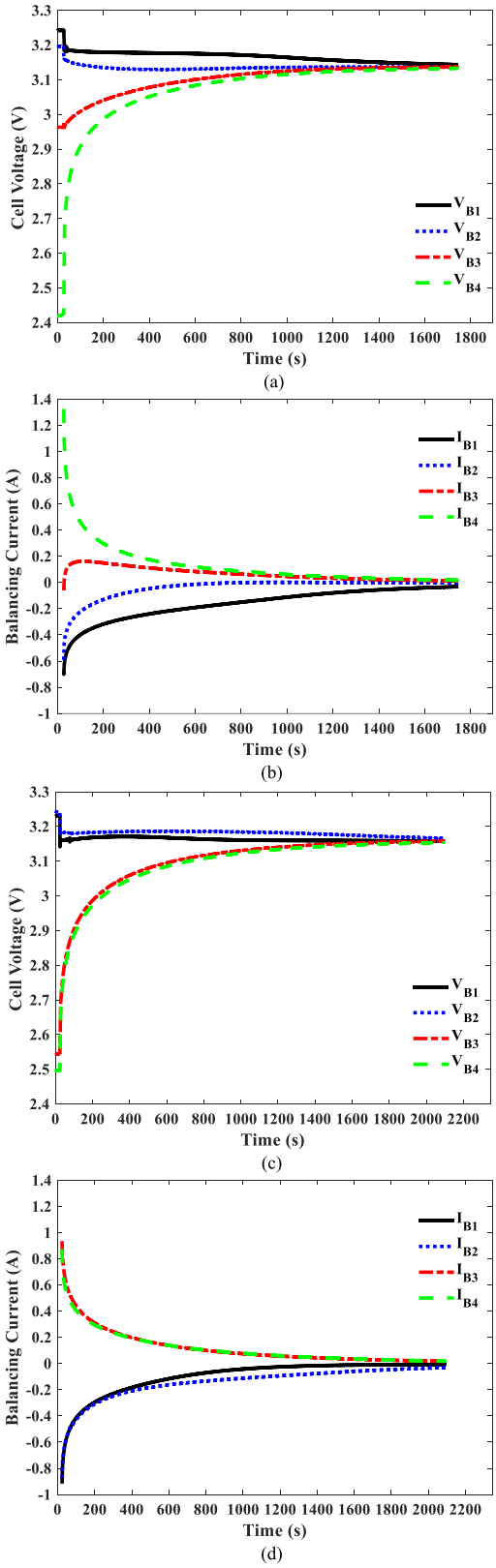

Fig. 8. Equalization performances of the proposed equalizer for four series-connected cells with different initial cell voltage distributions. (a) Cell voltage evolution with the initial voltage distribution of $V_{B1} > V_{B2} > V_{B3} > V_{B4}$. (b) Cell current evolution with the initial voltage distribution of $V_{B1} > V_{B2} > V_{B3} > V_{B4}$. (c) Cell voltage evolution with the initial voltage distribution of $V_{B2} > V_{B1} > V_{B3} > V_{B4}$. (d) Cell current evolution with the initial voltage distribution of $V_{B2} > V_{B1} > V_{B3} > V_{B4}$.

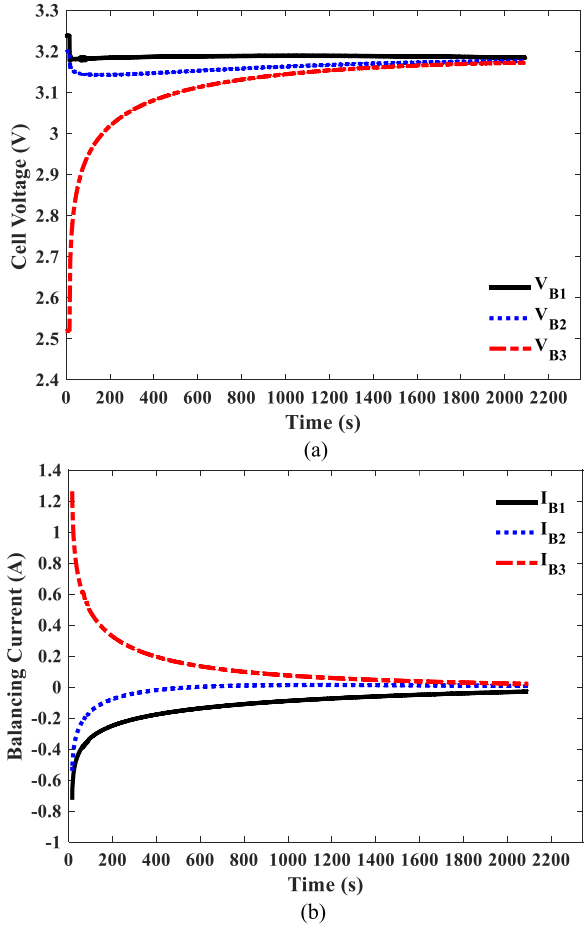

Fig. 9. Equalization performance of the proposed equalizer for odd series-connected cells. (a) Cell voltages. (b) Cell currents.

of Fig. 8(a). By comparison, we can conclude that the proposed equalizer has almost the same balancing speed as the conventional forward–flyback equalizer [26] in spite of the halved windings.

Fig. 11 further shows a comparison of the balancing currents and efficiencies of the proposed solution with the conventional forward–flyback equalizer [26]. It can be seen that the balancing current and efficiency of the proposed equalizer are slightly lower, i.e., by 0.2 A and 3%, than the forward–flyback equalizer [26] at larger balancing power. However, there is less difference in the balancing current and efficiency at smaller balancing power.

IV. Comparison With Conventional Transformer-Based Equalizers

In order to identify the advantages of the proposed equalizer, Table II illustrates a comparison of the transformer-based solutions in terms of the component number, circuit size, and total cost. It is assumed that the battery string includes 8 battery modules with 12 cells in 1 module. The total cost is calculated according to the quantity of the components and the component cost per unit. The size is evaluated according to the size of the components and the component number. It is important to note

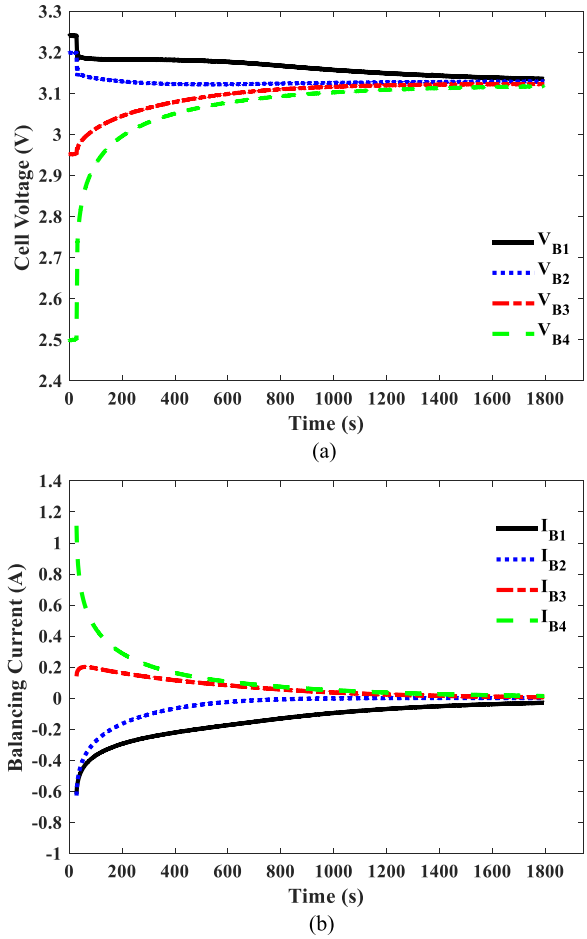

Fig. 10. Equalization performance of the conventional forward–flyback equalizer for four series-connected cells. (a) Cell voltages. (b) Cell currents.

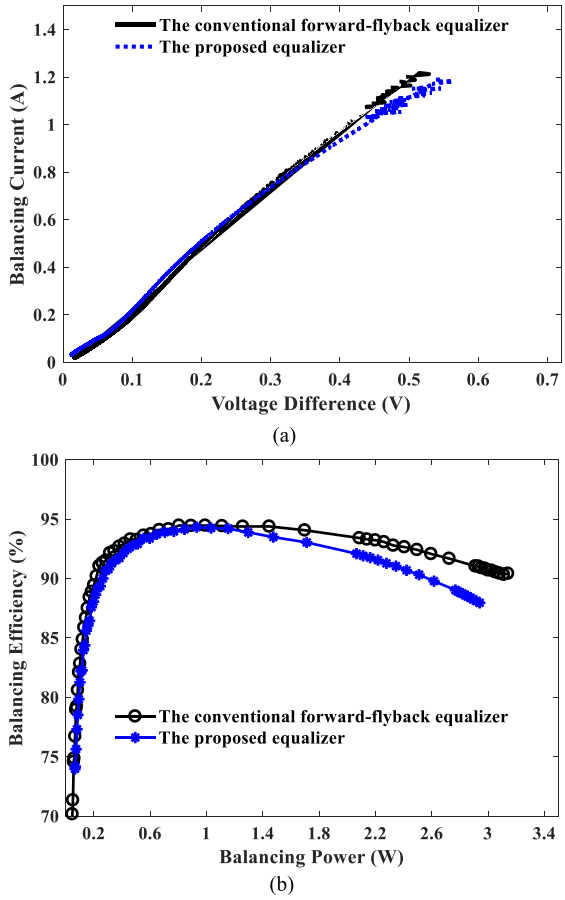

Fig. 11. Comparison of the balancing current and efficiency of the proposed equalizer with the conventional forward–flyback equalizer [26]. (a) Measured balancing currents. (b) Measured balancing efficiencies.

that in order to achieve a good consistency and small size, a multi-winding transformer has a maximum of six windings.

Furthermore, Table III presents a comparison in terms of the voltage stress on MOSFETs, balancing speed, current, efficiency, average winding power, and control. The balancing speed is evaluated by the balancing paths and the total balancing current for 12 series-connected cells. The balancing paths include the AC2C, DC2C, P2C, C2P, and AC2AC balancing methods. The control is evaluated according to whether or not the equalizer requires cell voltage monitoring.

As shown in Table II, the interleaved forward converter [14] uses 192 MOSFETs, 190 windings, and 95 magnetic cores for a 96-cell battery string, leading to a large size and high cost, i.e., \$277.5. Moreover, energy is only transferred from one cell to the adjacent cell with a slow equalization speed. The average balancing current is 2 A, causing a higher average power of a winding, i.e., 6.4 W. The advantages are the high balancing efficiency of 95%, low voltage stress on MOSFETs, and simple control.

The flyback or forward converter [16] uses 192 MOSFETs, 96 windings, and 16 magnetic cores, which also has a large size and high cost of \$219.2. This method realizes the DC2C equalization, but needs cell voltage monitoring, leading to a complex control. Particularly, the average power of a winding is up to 6.4 W. The advantages are the lower voltage stress on MOSFETs and high reliability.

Compared with the flyback or forward converter [16], the buck–boost and flyback converter [17] reduces the windings by half with the same equalization paths. Therefore, the total cost is reduced to \$205.6. Particularly, the balancing efficiency is up to 96%. The drawback is the DC2C equalization with a small balancing current of 0.5 A, leading to a slow balancing speed and a low winding power, i.e., 1.6 W.

The flyback converter [18] only needs 8 transformer windings, but requires 198 MOSFET switches to select the highest or lowest voltage cells, which has complex control. The total cost is at the medium level, i.e., \$205.2. Moreover, this method only transfers energy from the more-charged cell to the less-charged one with the average balancing current of 0.5 A, resulting in a slow equalization speed. Particularly, the MOSFETs are connected in parallel, which have a higher voltage stress, leading to a low reliability.

The time-shared flyback equalizer [19] only uses eight small transformers with two windings. However, this method employs 176 MOSFETs and 176 diodes to realize the C2P equalization with a 0.5 A balancing current. The total cost of this equalizer [19] is \$209.6, which is at an average level. Moreover, this solution needs a voltage monitoring circuit to select the highest

TABLE II
COMPARISON OF TRANSFORMER-BASED BATTERY EQUALIZERS IN TERMS OF COMPONENT NUMBER, SIZE, AND COST

Equalizers	Component number				Size	Cost ($)①	
	MOSFET	Diode	Winding	Magnetic core			
Interleaved forward converter [14]	192	0	190	95	Large	277.5	High
Flyback or forward converter [16]	192	0	96	16	Large	219.2	Medium
Buck-boost and flyback converter [17]	192	0	48	8	Small	205.6	Medium
Flyback converter [18]	198	0	16	8	Small	205.2	Medium
Time-shared flyback converter [19]	176	176	16	8	Small	209.6	Medium
Modularized flyback converter [21]	386	2	4	2	Small	388.1	High
Forward equalizer [15]	96	0	96	16	Medium	123.2	Low
Forward-flyback converter [26]	96	0	96	16	Medium	123.2	Low
Proposed equalizer	96	0	48	8	Small	109.6	Low

① Component cost per unit ($): MOSFET (0.2), MOSFET Driver IC (0.8), Diode (0.15), Winding (0.2), and Transformer Core (0.5) [19].

TABLE III
COMPARISON OF TRANSFORMER-BASED BATTERY EQUALIZERS IN TERMS OF BALANCING PERFORMANCES

Equalizers	MOSFET voltage stress	Balancing Speed		Balancing efficiency	Winding power	Control
Interleaved forward converter [14]	$2V_B$①	AC2C	2A	95%	6.4 W	Simple
Flyback or forward converter [16]	V_B	DC2C	2A	81%	6.4 W	Complex
Buck-boost and flyback converter [17]	V_B	DC2C	0.5A	Unavailable	1.6 W	Complex
Flyback converter [18]	$5.5V_B$	DC2C	0.5A	96%	1.6 W	Complex
Time-shared flyback converter [19]	$11V_B$	C2P	0.5A	88%	0.6 W	Complex
Modularized flyback converter [21]	$96V_B$	P2C,C2P	2A	82%	6.4 W	Complex
Forward equalizer [15]	V_B	AC2AC	1.8A	93%	1.0 W	Simple
Forward-flyback converter [26]	V_B	AC2AC	2.5A	95%	1.3 W	Simple
Proposed equalizer	V_B	AC2AC	2.3A	95%	2.5 W	Simple

① V_B is the cell voltage.

voltage cell, whose control is more complex than the automatic equalizers.

The modularized flyback converter [21] achieves the P2C and C2P equalization using two small transformers with a 2 A balancing current. However, 6.4 W windings and 386 MOSFETs with the withstand voltage of $96V_B$ are required, leading to a large volume, high cost of $388.1, and low reliability. Moreover, the equalization efficiency is lower, i.e., 82%, because of the unnecessary energy loss of the P2C and C2P equalization.

The forward equalizer [15] only uses 96 MOSFETs, 96 windings, and 16 cores to achieve the fast-speed AC2AC equalization with a high efficiency of 93% and a large total current of 1.8 A. Because the balancing power distributes averagely in all windings, the average power of each winding is only 1.0 W. It is worth noting that the total cost is only $123.2 and the control is very simple with one PWM signal. However, this method needs additional demagnetizing circuits, leading to complex design and low reliability.

The forward–flyback converter [26] is an improvement of the forward equalizer [15], which removes the demagnetizing circuits with the same MOSFET and winding numbers. In addition, this method has also the advantages, i.e., low cost of $123.2, low voltage stress on MOSFETs, large balancing current of 2.5 A, low winding power of 1.3 W, and high efficiency of 95%.

In fact, the proposed equalizer is a further improvement of the forward–flyback converter [26], which reduces the windings by half based on forward, flyback, and buck–boost operations. It is worth mentioning that in spite of the halved windings, the proposed equalizer has almost the same equalization performances as the forward–flyback converter [26], e.g., the AC2AC equalization with 2.4 A average balancing current, 95% efficiency, and low voltage stress on MOSFETs. Due to the reduced windings and low voltage stress on MOSFETs, the proposed equalizer has the most compact size and lowest cost, i.e., $109.6. The only drawback is that the average power of each winding is 2.5 W, which is higher than the forward–flyback converter [26], i.e., 1.3 W, but is lower than the conventional AC2C and DC2C transformer-based equalizers, i.e., 6.4 W.

V. CONCLUSION

This paper proposed an optimized equalizer based on coupled half-bridge converters, which reduced the transformer windings by half. An experimental prototype for four series-connected cells was built. The analytical expressions of the balancing currents were derived and verified by experiments. The balancing current and efficiency were analyzed and discussed at different switching frequencies and magnetic inductances. Comparative experimental studies of the proposed optimized equalizer with the forward–flyback solution [26] were conducted.

Analyses and experimental results demonstrated the following.

1) The balancing current is mainly decided by the voltage difference, equivalent resistance, leakage inductance, and switching frequency, but independent of the magnetic inductance.
2) Decreasing the switching frequency with a fixed magnetic inductance can significantly improve the balancing current.
3) Increasing the magnetic inductance at the same switching frequency can effectively improve the balancing efficiency.
4) Due to the conduction, core, and switching losses, there is an optimized switching frequency to maximize the balancing efficiency.
5) Comparative experimental results show that the proposed topology has almost the same equalization speed, current, and efficiency as the conventional forward–flyback solution [26] in spite of the halved windings.

REFERENCES

[1] J. Gallardo-Lozano, E. Romero-Cadaval, M. I. Milanes-Montero, and M. A. Guerrero-Martinez, "Battery equalization active methods," *J. Power Sources*, vol. 246, pp. 934–949, 2014.

[2] M. Uno and K. Tanaka, "Single-Switch multioutput charger using voltage multiplier for series-connected lithium-ion battery/supercapacitor equalization," *IEEE Trans. Ind. Electron.*, vol. 60, no. 8, pp. 3227–3239, Aug. 2013.

[3] T. Anno and H. Koizumi, "Double-Input bidirectional DC/DC converter using cell-voltage equalizer with flyback transformer," *IEEE Trans. Power Electron.*, vol. 30, no. 6, pp. 2923–2934, Jun. 2015.

[4] Z. Zhang, H. Gui, D.-J. Gu, Y. Yang, and X. Ren, "A hierarchical active balancing architecture for lithium-ion batteries," *IEEE Trans. Power Electron.*, vol. 32, no. 4, pp. 2757–2768, Apr. 2017.

[5] Y. Shang, C. Zhu, Y. Fu, and C. Mi, "An integrated heater-equalizer for lithium-ion batteries of electric vehicles," *IEEE Trans. Ind. Electron.*, to be published, doi:10.1109/TIE.2018.2863187.

[6] C. Pascual and P. T. Krein, "Switched capacitor system for automatic series battery equalization," in *Proc. IEEE Appl. Power Electron. Conf.*, 1997, pp. 848–854.

[7] Y. Ye and K. W. E. Cheng, "Modeling and analysis of series-parallel switched-capacitor voltage equalizer for battery/supercapacitor strings," *IEEE J. Emerg. Sel. Topics Power Electron.*, vol. 3, no. 4, pp. 977–983, Dec. 2015.

[8] Y. Ye, K. W. E. Cheng, Y. C. Fong, X. Xue, and J. Lin, "Topology, modeling, and design of switched-capacitor-based cell balancing systems and their balancing exploration," *IEEE Trans. Power Electron.*, vol. 32, no. 6, pp. 4444–4454, Jun. 2017.

[9] Y. Shang, B. Xia, F. Lu, C. Zhang, N. Cui, and C. Mi, "A switched-coupling-capacitor equalizer for series-connected battery strings," *IEEE Trans. Power Electron.*, vol. 32, no. 10, pp. 7694–7706, Oct. 2017.

[10] Y. Ye, K. W. E. Cheng, and Y. P. B. Yeung, "Zero-Current switching switched-capacitor zero-voltage-gap automatic equalization system for series battery string," *IEEE Trans. Power Electron.*, vol. 27, no. 7, pp. 3234–3242, Jul. 2012.

[11] K. Lee, Y. Chung, C.-H. Sung, and B. Kang, "Active cell balancing of Li-ion batteries using LC series resonant circuit," *IEEE Trans. Ind. Electron.*, vol. 62, no. 9, pp. 5491–5501, Sep. 2015.

[12] F. Mestrallet, L. Kerachev, J.-C. Crebier, and A. Collet, "Multiphase interleaved converter for lithium battery active balancing," *IEEE Trans. Power Electron.*, vol. 29, no. 6, pp. 2874–2881, Jun. 2014.

[13] M.-Y. Kim, J.-H. Kim, and G.-W. Moon, "Center-Cell concentration structure of a cell-to-cell balancing circuit with a reduced number of switches," *IEEE Trans. Power Electron.*, vol. 29, no. 10, pp. 5285–5297, Oct. 2014.

[14] T. H. Phung, A. Collet, and J.-C. Crebier, "An optimized topology for next-to-next balancing of series-connected lithium-ion cells," *IEEE Trans. Power Electron.*, vol. 29, no. 9, pp. 4603–4613, Sep. 2014.

[15] S. Li, C. Mi, and M. Zhang, "A high-efficiency active battery-balancing circuit using multiwinding transformer," *IEEE Trans. Ind. Appl.*, vol. 49, no. 1, pp. 198–207, Jan. 2013.

[16] Y. Chen, X. Liu, Y. Cui, J. Zou, and S. Yang, "A multi-winding transformer cell-to-cell active equalization method for lithium-ion batteries with reduced number of driving circuits," *IEEE Trans. Power Electron.*, vol. 31, no. 7, pp. 4916–4929, Jul. 2016.

[17] S.-H. Park, K.-B. Park, H.-S. Kim, G.-W. Moon, and M.-J. Youn, "Single-Magnetic cell-to-cell charge equalization converter with reduced number of transformer windings," *IEEE Trans. Power Electron.*, vol. 27, no. 6, pp. 2900–2911, Jun. 2012.

[18] K.-M. Lee, S.-W. Lee, Y.-G. Choi, and B. Kang, "Active balancing of Li-Ion battery cells using transformer as energy carrier," *IEEE Trans. Ind. Electron.*, vol. 64, no. 2, pp. 1251–1257, Feb. 2017.

[19] A. M. Imitiaz and F. H. Khan, ""Time shared flyback converter" based regenerative cell balancing technique for series connected Li-Ion battery strings," *IEEE Trans. Power Electron.*, vol. 28, no. 12, pp. 5960–5975, Dec. 2013.

[20] M. Arias, J. Sebastián, M. Hernando, U. Viscarret, and I. Gil, "Practical application of the wave-trap concept in battery-cell equalizers," *IEEE Trans. Power Electron.*, vol. 30, no. 10, pp. 5616–5631, Oct. 2015.

[21] C.-H. Kim, M.-Y. Kim, and G.-W. Moon, "A modularized charge equalizer using a battery monitoring IC for series-connected Li-Ion battery strings in electric vehicles," *IEEE Trans. Power Electron.*, vol. 28, no. 8, pp. 3779–3787, Aug. 2013.

[22] C.-H. Kim, M.-Y. Kim, H.-S. Park, and G.-W. Moon, "A modularized two-stage charge equalizer with cell selection switches for series-connected lithium-ion battery string in an HEV," *IEEE Trans. Power Electron.*, vol. 27, no. 8, pp. 3764–3774, Aug. 2012.

[23] C.-S. Lim, K.-J. Lee, N.-J. Ku, D.-S. Hyun, and R.-Y. Kim, "A modularized equalization method based on magnetizing energy for a series-connected Lithium-Ion battery string," *IEEE Trans. Power Electron.*, vol. 29, no. 4, pp. 1791–1799, Apr. 2014.

[24] M. Uno and A. Kukita, "Double-Switch equalizer using parallel-or series-parallel-resonant inverter and voltage multiplier for series-connected supercapacitors," *IEEE Trans. Power Electron.*, vol. 29, no. 2, pp. 812–828, Feb. 2014.

[25] L. McCurlie, M. Preindl, and A. Emadi, "Fast model predictive control for redistributive lithium ion battery balancing," *IEEE Trans. Ind. Electron.*, vol. 64, no. 2, pp. 1350–1357, Feb. 2017.

[26] Y. Shang, B. Xia, C. Zhang, N. Cui, J. Yang, and C. Mi, "An automatic equalizer based on forward-flyback converter for series-connected battery strings," *IEEE Trans. Ind. Electron.*, vol. 64, no. 7, pp. 5380–5391, Jul. 2017.

[27] Y. Shang, B. Xia, C. Zhang, N. Cui, J. Yang, and C. Mi, "A modularization method for battery equalizers using multi-winding transformers," *IEEE Trans. Veh. Technol.*, vol. 66, no. 10, pp. 8710–8722, Oct. 2017.

[28] E. C. Snelling, *Soft Ferrites, Properties and Applications*, 2nd Ed. London, U.K.: Butterworth, 1988.

[29] W. A. Roshen, "A practical, accurate and very general core loss model for nonsinusoidal waveforms," *IEEE Trans. Power Electron.*, vol. 22, no. 1, pp. 30–40, Jan. 2007.

[30] Y. Ren, M. Xu, J. Zhou, and F. C. Lee, "Analytical loss model of power MOSFET," *IEEE Trans. Power Electron.*, vol. 21, no. 2, pp. 310–319, Mar. 2013.

[31] D. Gravoac, M. Purschel, and A. Kiep, "MOSFET power losses calculation using the data-sheet parameters," Infineon, Neubiberg, Germany, Appl. Note, vol. 1.1, Jul. 2006.

Yunlong Shang (S'14–M'18) received the B.S. degree in automation from the Hefei University of Technology, Hefei, China, in 2008, and the Ph.D. degree in control theory and control engineering from Shandong University, Jinan, China, in 2017.

Between September 2015 and October 2017, he conducted scientific research as a joint Ph.D. student with the DOE GATE Center for Electric Drive Transportation and the Department of Electrical and Computer Engineering, San Diego State University, San Diego, CA, USA, where since 2017, he has been a Postdoctoral Research Fellow. His current research interests include battery balancing, self-heating, modeling, states estimation, and design of battery management systems. He wined the excellent doctoral dissertation award of Chinese Association of Automation (CAA) in 2018.

Naxin Cui (M'14–SM'18) received the B.S. degree in automation from Tianjin University, Tianjin, China, in 1989, and the M.S. and Ph.D. degrees in control theory and applications from Shandong University, Jinan, China, in 1994 and 2005, respectively.

In 1994, she joined Shandong University, where she is currently a Full Professor with the School of Control Science and Engineering. Between December 2016 and February 2017, she conducted scientific research as a Visiting Scholar in the DOE GATE Center for Electric Drive Transportation, San Diego State University, San Diego, CA, USA. Her current research interests include power electronics, motor drives, automatic control theory and application, and battery energy management system of electric vehicles.

Chenghui Zhang (M'14–SM'17) received the bachelor's and master's degrees in automation engineering from the Shandong University of Technology, Jinan, China, in 1985 and 1988, respectively, and the Ph.D. degree in control theory and operational research from Shandong University, Jinan, in 2001, respectively.

In 1988, he joined Shandong University, where he is currently a Professor with the School of Control Science and Engineering, Shandong University, the Chief Manager with the Power Electronic Energy-saving Technology & Equipment Research Center of Education Ministry, a Specially Invited Cheung Kong Scholars Professor by China Ministry of Education, and a Taishan Scholar Special Adjunct Professor. He is also one of the state-level candidates of the "New Century National Hundred, Thousand and Ten Thousand Talent Project," the Academic Leader of Innovation Team of Ministry of Education, and the Chief Expert of the National "863" high technological planning. His research interests include optimal control of engineering, power electronics and motor drives, energy-saving techniques, and time-delay systems.